Unified quantifier of mechanical disorder in solids

Kapteijns, G.; Bouchbinder, E.; Lerner, E.

Link to publication

Unified quantifier of mechanical disorder in solids

Geert Kapteijns [1,*] Eran Bouchbinder [2,†] and Edan Lerner [1,‡]

[1]*Institute of Theoretical Physics, University of Amsterdam, Science Park 904, 1098 XH Amsterdam, the Netherlands*
[2]*Chemical and Biological Physics Department, Weizmann Institute of Science, Rehovot 7610001, Israel*

Mechanical disorder in solids, which is generated by a broad range of physical processes and controls various material properties, appears in a wide variety of forms. Defining unified and measurable dimensionless quantifiers, allowing quantitative comparison of mechanical disorder across widely different physical systems, is therefore an important goal. Two such coarse-grained dimensionless quantifiers (among others) appear in the literature: one is related to the spectral broadening of discrete phononic bands in finite-size systems (accessible through computer simulations) and the other is related to the spatial fluctuations of the shear modulus in macroscopically large systems. The latter has been recently shown to determine the amplitude of wave attenuation rates in the low-frequency limit (accessible through laboratory experiments). Here, using two alternative and complementary theoretical approaches linked to the vibrational spectra of solids, we derive a basic scaling relation between the two dimensionless quantifiers. This scaling relation, which is supported by simulational data, shows that the two apparently distinct quantifiers are in fact intrinsically related, giving rise to a unified quantifier of mechanical disorder in solids. We further discuss the obtained results in the context of the unjamming transition taking place in soft sphere packings at low confining pressures, in addition to their implications for our understanding of the low-frequency vibrational spectra of disordered solids in general, and in particular those of glassy systems.

I. INTRODUCTION

Mechanical disorder in solids appears in a multitude of forms, e.g., manifested in the material's composition, in the spatial arrangement of its constituents, and in the interactions between them. It can be generated by a broad range of physical processes, taking place either during solid formation (e.g., solidification or glass transition [1]) and/or after it (e.g., through various heat treatments [2], irreversible mechanical deformation [3], and irradiation [4]). Mechanical disorder has a deep impact on the properties of solids, such as stress relaxation [5], sound attenuation [6–8], thermal conductivity [9], plastic deformability [10], and failure resistance [11–13]. Consequently, quantifying mechanical disorder is important; in particular, it is highly desirable to define measurable dimensionless and universally applicable quantifiers of mechanical disorder, which allow us to quantitatively compare the degree of disorder of widely different physical systems [14–16].

Several proposals of quantifiers of *mechanical* disorder exist in the literature [14,15,17–27]. Of particular relevance in the present context are measurable disorder quantifiers that play key roles in determining material properties and that can be applied in both computer simulations—that are playing increasingly important roles in materials research due to the dramatic rise in computing power—and in laboratory experiments. As such, the disorder quantifiers we consider are coarse grained to some extent, probing the effect of disorder on some measurable physical properties. One such quantifier can be constructed using the standard deviation of the spatial distribution of the shear modulus μ, denoted by $\Delta\mu$. The ratio $\Delta\mu/\langle\mu\rangle$ (where $\langle\mu\rangle$ is the average shear modulus, cf. Fig. 1) can be used to define a dimensionless disorder quantifier. Such a definition can make physical sense only if it is scale independent, i.e., if the spatial fluctuations of μ are probed on a length scale ℓ such that $(\Delta\mu/\langle\mu\rangle)(\ell/a_0)^{d/2}$ is independent of ℓ. Here d is the spatial dimension, a_0 is an atomistic length, and ℓ is larger than any possible correlation length associated with the spatial fluctuations of μ. This disorder quantifier plays a central role in a class of theoretical approaches collectively termed Fluctuating Elasticity Theory (FET) [14,17–20], which was recently shown to control wave attenuation rates in disordered solids [8] and to correlate with the number density of soft, quasilocalized modes in structural glasses [13]. Its precise definition and ways to probe it will be discussed in detail below.

Another quantifier of mechanical disorder has been related to the spectral broadening of low-frequency phononic bands in solids [25]. Low-frequency phonons exist in solids due to a broken global continuous symmetry, independently of whether the solids are ordered (e.g., crystalline) or disordered. For finite-size solids, lowest-frequency phonons appear in well-separated, discrete bands. If the solid is ordered, the discrete phononic bands are degenerate, i.e., groups of phonons with different wave vectors share the same frequency ω. In the presence of mechanical disorder, this degeneracy is lifted

*g.h.kapteijns@uva.nl
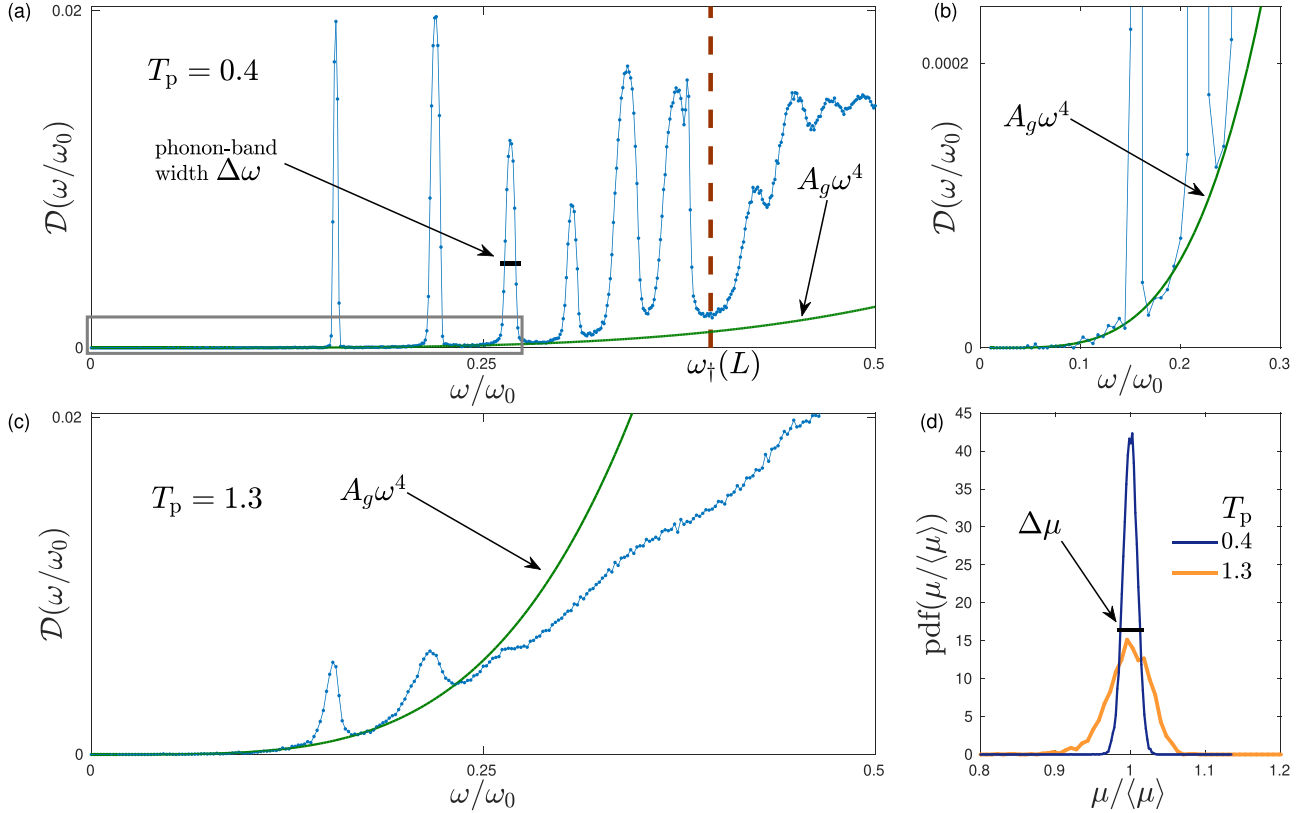†eran.bouchbinder@weizmann.ac.il
‡e.lerner@uva.nl

FIG. 1. (a)–(c) Low-frequency density of states $\mathcal{D}(\omega)$ averaged over 100 computer glasses of $N = 64\,000$ particles in three dimensions, plotted against the rescaled frequency ω/ω_0, where $\omega_0 \equiv c_s/a_0$ with c_s the (ensemble averaged, T_p-dependent) speed of shear waves, and $a_0 \equiv (V/N)^{1/3}$ is an interparticle distance in a system of volume V. (a) Data for glasses of parent temperature $T_\text{p} = 0.4$ (in simulational units); the disorder-dependent frequency scale $\omega_\dagger(L)$ indicated by the dashed vertical line separates the frequency axis into the range in which discrete phonon bands are distinguishable, and the range in which their width surpasses the gaps between them, rendering them indistinguishable (phonon sea). The grey rectangle indicates the zoomed-in window presented in panel (b), where the universal $\sim\omega^4$ VDoS of nonphononic modes is observed between and below the discrete phonon bands. (c) Same as (a) but for $T_\text{p} = 1.3$ glasses of larger mechanical disorder. The dimensionless prefactor $A_g\omega_0^5$ is roughly 35 times larger compared to the $T_\text{p} = 0.4$ glasses. (d) Sample-to-sample probability distribution functions (PDFs) of the shear modulus μ, measured for $T_\text{p} = 1.3$ and $T_\text{p} = 0.4$ glasses of $N = 16\,000$ particles.

and the discrete phononic bands acquire a finite spectral width $\Delta\omega$, as demonstrated in Fig. 1. Consequently, $\Delta\omega/\omega$ can be used to construct a dimensionless disorder quantifier. The precise definition based on $\Delta\omega/\omega$ and ways to probe it will be discussed in detail below. The main questions we aim at addressing in this paper are whether the disorder quantifier defined based on $\Delta\mu/\langle\mu\rangle$ is fundamentally related to the one defined based on $\Delta\omega/\omega$, and if so, what the physical content and meaning of such a basic relation are.

To better understand these questions and to sharpen them, we present in Fig. 1(a) the low-frequency vibrational density of states $\mathcal{D}(\omega)$ (VDoS) of finite-size computer glasses comprised of $N = 64\,000$ particles in three dimensions, obtained by quenching a deeply supercooled equilibrium liquid to zero temperature (details about the model and methods are provided below). It is observed that phononic bands localized at discrete frequencies exist at the lowest tail of the VDoS [28]. Each phononic band is also characterized by a well-defined width $\Delta\omega$, explicitly marked on the third band for illustration, making the ratio $\Delta\omega/\omega$ well defined for each band. The lowest phononic bands are shown to be superimposed on top of an ω^4 function (continuous green line), as highlighted by the

zoom-in view presented in Fig. 1(b). The ω^4 law corresponds to nonphononic excitations, which have been recently shown to be a universal feature of glasses formed by quenching a melt [16,29–32]. As the nonphononic part of the VDoS universally follows the ω^4 law, the prefactor A_g of this law (see figure) encapsulates nonuniversal properties of the glass and, in particular, must be sensitive to the degree of mechanical disorder, which depends on the glass preparation procedure [24,26,32].

At higher frequencies, the VDoS changes its character. In particular, when a crossover frequency $\omega_\dagger$ (which depends on the linear system size L, as well as on the disorder quantifier χ as explained below) is surpassed, discrete phononic bands are no longer clearly distinguishable [25]. Moreover, the ω^4 law of nonphononic excitations is not clearly observed due to the overwhelming abundance of phonons, which eventually (at frequencies $\omega > \omega_\dagger$) follow Debye's density of states $\sim\omega^{d-1}$ in d spatial dimensions (not shown). In these terms, the posed challenge is to understand how $\Delta\mu/\langle\mu\rangle$ manifests itself within the phonon sea for $\omega > \omega_\dagger$ and how it might be related to the spectral broadening of discrete phononic bands at $\omega < \omega_\dagger$. If this challenge is met, then one is able

to unify two apparently distinct dimensionless quantifiers of mechanical disorder, which are accessible in both finite-size computer solids and in macroscopically large solids. In the latter context, one should also establish experimental procedures to probe the disorder quantifier.

In this paper, a basic relation between the two mechanical disorder quantifiers discussed above is derived and substantiated through computer simulations. The former is achieved using two alternative and complementary theoretical approaches that intimately link mechanical disorder to the low-frequency vibrational spectra of solids and to its effect on wave attenuation in such systems. The relation to low-frequency vibrational spectra, following FET [14,17–20] and the very recent support it received [8], makes the emerging unified disorder quantifier experimentally accessible using techniques such as neutron and inelastic x-ray scattering.

To robustly validate the derived relation between the two mechanical disorder quantifiers against computer simulations, we seek to study model systems that feature the largest-possible range of mechanical disorder. To this aim, we employed a glass-forming model [33] that can be very deeply supercooled using the swap-Monte-Carlo method [34,35]. In addition, the unified disorder quantifier is applied to packings near the unjamming transition and to disordered elastic spring-networks at low connectivities; as discussed in what follows, the mechanical disorder in these systems can vary substantially by driving them to the unjamming point [36,37].

Consequently, our work theoretically and computationally substantiates a unified quantifier of mechanical disorder in solids, thus allowing us to quantify mechanical disorder across widely different physical systems using various probing techniques. At the same time, it offers insight into the low-frequency vibrational spectra of disordered solids in general and, in particular, those of glassy systems.

II. OBSERVABLES AND THEORY

In this section, we introduce and relate two broadly applicable quantifiers of mechanical disorder, both illustrated in Fig. 1. The first quantifier, χ, is related to the spectral broadening of discrete phonon bands that emerge at the lowest frequencies of the vibrational spectrum of finite-size solids, as marked in Fig. 1(a). The second quantifier is known as the disorder parameter γ [14,17–20] and is related to the relative width of the spatial or sample-to-sample [38] distribution of the shear modulus μ, as shown, for example, in Fig. 1(d).

A. The mechanical-disorder quantifier χ

Phonons are collective, wavelike excitations that emerge in solids due to global translational symmetry [39]. In an ideal homogeneous and isotropic linear-elastic medium, phonons that share the same wavelength feature the exact same vibrational frequency, if they are also of the same polarization (shear or sound waves). This frequency degeneracy of phonons, expected in ideal continua, is lifted in disordered solids due to structural and mechanical disorder [25]. Consequently, ideal phononic modes of a particular wave vector $\boldsymbol{k}$ and frequency ω feature sizable projections on eigenvectors (normal modes) of the disordered system that are character-

ized by a frequency range $\Delta\omega$. We hereafter refer to $\Delta\omega$, which corresponds to the spectral width of the dynamic structure factor at a wave vector $\boldsymbol{k}$, as the *spectral width* pertaining to wave vector $\boldsymbol{k}$. In an isotropic solid, the spectral widths depend on the magnitude $k \equiv |\boldsymbol{k}|$ (in addition to other observables, see below); in what follows, we restrict the discussion to isotropic media.

How does the spectral width $\Delta\omega(k)$ depend on k? At the smallest allowed phonon frequencies of a solid of linear size L, the spectral widths $\Delta\omega(k)$ are smaller than the frequency gaps between phonons of successive allowed wave vectors, i.e., they remain *discrete*, as is clearly shown in Fig. 1(a). Sorting the low-frequency, discrete phonon bands by increasing wave vectors k, we denote the phonon band index by z, and the (lifted) degeneracy of the zth band by n_z. The latter is given by the number of *different* solutions to the sum-of-integer-squares problem, namely, the number of different combinations of integers m_x, m_y, m_z such that

$$m_x^2 + m_y^2 + m_z^2 = z. \tag{1}$$

Notice that the wave vector $\boldsymbol{k}$ is related to the integers $\boldsymbol{m} \equiv (m_x, m_y, m_z)$ as $\boldsymbol{k} = (2\pi/L)\boldsymbol{m}$ [39], and $|\boldsymbol{m}| = \sqrt{z}$.

In Ref. [25], a perturbation theory was developed, culminating in a prediction for the scaling behavior of the spectral widths of discrete phonon bands; it reads [25]

$$\Delta\omega(\omega, z, N) \propto \frac{\omega\sqrt{n_z}}{\sqrt{N}}, \tag{2}$$

where N is the system size, $\omega \simeq ck$ is the frequency of phonons from the zth band (c is the wave speed), and n_z is their (lifted) degeneracy level. The prefactor of this proportionality relation defines a dimensionless mechanical disorder quantifier χ, namely [25],

$$\chi \equiv \frac{\Delta\omega(\omega, z, N)\sqrt{N}}{\omega\sqrt{n_z}}. \tag{3}$$

Figures 1(a) and 1(c) present the low-frequency VDoS of computer glasses of $N = 64\,000$ quenched from different equilibrium parent temperatures T_p (as indicated by the legends); the different degrees of mechanical disorder featured by these glasses is manifested in the much-larger spectral widths $\Delta\omega$ of the high-T_p glasses.

B. The phonon sea crossover frequency $\omega_\dagger$

Equation (2) for the spectral widths of discrete phonon bands holds up to a system-size dependent crossover frequency scale $\omega_\dagger(L)$, defined by the condition that the spectral width of discrete phonon bands becomes comparable to the gaps between successive phonon bands. Incorporating the definition of χ spelled out above and following Ref. [25], the crossover frequency $\omega_\dagger$ is predicted to satisfy [25]

$$\omega_\dagger \sim (\chi L)^{-\frac{2}{d+2}}, \tag{4}$$

where d again denotes the dimension of space. $\omega_\dagger$ is marked by the vertical line in the example of Fig. 1(a), and its scaling with L was validated using numerical simulations in Ref. [40]. At frequencies $\omega > \omega_\dagger$, discrete phonon bands are no longer distinguishable, and a phonon sea emerges instead, as seen in

Figs. 1(a) and 1(c). Since $\omega_\dagger \to 0$ in the thermodynamic limit, the phonon sea is expected to extend to zero frequency in that limit. In the phonon sea, Debye's VDoS [39] for phonon frequencies $\mathcal{D}(\omega) \sim \omega^{\bar{d}-1}$ is expected to hold.

C. Spectral widths in the phonon sea

How do the spectral widths $\Delta\omega(k)$ behave at frequencies $\omega > \omega_\dagger$, deep inside the phonon sea? Let us assume that Eq. (2) for the spectral width of discrete phonon bands with $\omega < \omega_\dagger$ also holds in the phonon sea; since the (lifted) degeneracy of phonons is no longer relevant (phonon bands are no longer discrete and well-separated in frequency), now n_z represents the *number* of modes that exist within the spectral widths $\Delta\omega$ (recall the physical meaning of the latter, as discussed above). n_z can therefore be related to the VDoS $\mathcal{D}(\omega)$ via [40]

$$n_z \simeq N\mathcal{D}(\omega)\Delta\omega. \tag{5}$$

Using this relation together with Eq. (2), we obtain

$$\Delta\omega \simeq \chi^2 \omega^2 \mathcal{D}(\omega), \tag{6}$$

which, importantly, is independent of the system size N. Equation (6) is closely related to the Rayleigh-Klemens law [41]. In the thermodynamic limit, we expect phonons to dominate the low-frequency spectrum [25], namely, $\mathcal{D}(\omega) \sim \omega_0^{-\bar{d}}\omega^{\bar{d}-1}$; we thus obtain the spectral widths inside the phonon sea in the form

$$\Delta\omega \sim \chi^2 \omega_0^{-\bar{d}} \omega^{\bar{d}+1}. \tag{7}$$

In the context of the attenuation rate of plane waves in disordered media, the $\sim\omega^{\bar{d}+1}$ scaling is known as Rayleigh scattering [42], and has been observed in numerical simulations in recent years [6,8,40,43,44].

D. The disorder parameter γ

FET [14,17–20] is a theoretical framework that relates the spatial fluctuations of the local elastic moduli fields of a disordered solid to its vibrational and thermodynamic properties. Of particular interest here is the low-frequency wave attenuation rate Γ, which according to FET scales as $\gamma\omega_0^{-\bar{d}}\omega^{\bar{d}+1}$, where γ is called the 'disorder parameter' defined as

$$\gamma \equiv \left(\frac{\Delta\mu}{\langle\mu\rangle}\right)^2\left(\frac{\ell}{a_0}\right)^{\bar{d}}. \tag{8}$$

Here ℓ represents the coarse-graining length on which the spatial fluctuations $\Delta\mu$ of the shear modulus are evaluated and a_0 is an interparticle length as defined above. Assuming that the spatial distribution of the shear modulus field is correlated on a length scale $\xi_g < \ell$, one expects the variance $(\Delta\mu)^2$ to scale as $\sim\ell^{-\bar{d}}$, and therefore γ should become independent of the coarse-graining length ℓ for large enough ℓ. Since we expect Γ to be proportional to $\Delta\omega$, we conclude that the spectral width $\Delta\omega$ at frequency ω follows

$$\Delta\omega \propto \gamma\omega_0^{-\bar{d}}\omega^{\bar{d}+1}. \tag{9}$$

E. A unified quantifier of mechanical disorder

Combining now Eqs. (7) and (9), we immediately conclude that

$$\chi^2 \sim \gamma, \tag{10}$$

which is the main result of this paper.

The very same result can be obtained based on Eqs. (2) and (9) alone; recall that the degeneracy $n_z(k)$ of wave vectors of magnitude k (for a perfectly homogeneous solid) is proportional to $k^{\bar{d}-1}$ [39], and that $k \sim \sqrt{z}/L$. Therefore, $n_z \sim z^{\frac{\bar{d}-2}{2}} \sim L^{\bar{d}-2}\omega^{\bar{d}-2}$ [25], and hence for large z phonon bands (at frequencies $\omega < \omega_\dagger$), we expect

$$\Delta\omega \sim \frac{\chi\omega^{\bar{d}/2}}{L}. \tag{11}$$

Requiring that the spectral widths for $\omega < \omega_\dagger$ smoothly connect to the spectral widths at $\omega > \omega_\dagger$ as given by Eq. (4), we obtain

$$\chi\frac{\omega_\dagger^{\bar{d}/2}}{L} \sim \gamma\omega_\dagger^{\bar{d}+1} \quad\Rightarrow\quad \omega_\dagger \sim \left(\frac{\gamma L}{\chi}\right)^{-\frac{2}{\bar{d}+2}}. \tag{12}$$

Comparing this result with the scaling relation for $\omega_\dagger$ in Eq. (4), we obtain

$$(\chi L)^{-\frac{2}{\bar{d}+2}} \sim \left(\frac{\gamma L}{\chi}\right)^{-\frac{2}{\bar{d}+2}} \quad\Rightarrow\quad \chi^2 \sim \gamma, \tag{13}$$

in agreement with Eq. (10) above.

III. NUMERICAL SUPPORT

Our goal in this section is to test our main prediction in Eq. (10) for computer glasses generated over a broad range of conditions, which mimic a correspondingly large range of cooling rates through the glass transition.

A. Models and methods

In this paper, we employ a computer glass model of highly polydispersed soft spheres interacting via a $\propto r^{-10}$ pairwise potential, where r is the distance between the centers of pairs of soft spheres. A full description of the model can be found in Ref. [45]. The model is inspired by the one put forward in Ref. [33], and as such it can be equilibrated down to very low temperatures using the swap-Monte-Carlo algorithm, where the latter is also explained in detail in Ref. [33]. The crossover temperature of this system is found to be $T_X \approx 0.66$ in the model's simulation units (as described in Ref. [45]), according to the definition introduced in Ref. [46]. T_X coincides with the onset of the high-T_p plateau of γ as shown in Fig. 3 below. The high-T_p shear modulus of this system is $\mu_\infty \approx 9.2$ in the model's simulation units.

We created ensembles of glassy samples of $N = 16\,000$ particles, parameterized by the equilibrium parent temperature T_p, from which liquid configurations were instantaneously quenched using a conventional minimization algorithm. The sample-to-sample fluctuations of the shear modulus were evaluated using ensembles of 2000 independent glassy samples for each T_p. We also created a similar set of glass ensembles with $N = 2000$ particles to demonstrate the
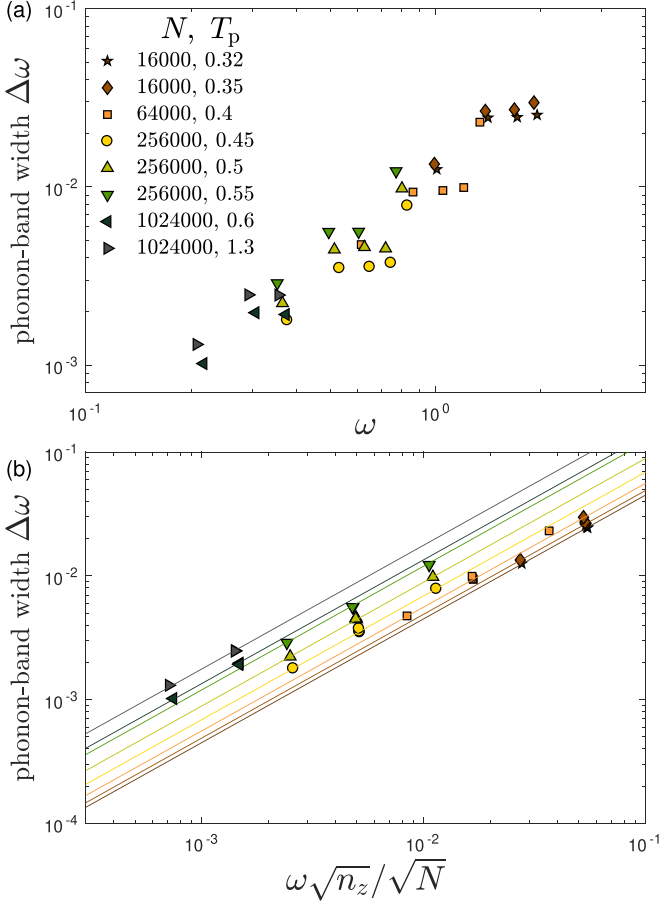
FIG. 2. (a) Phonon-band widths $\Delta\omega$ plotted against phonon bands frequencies ω (expressed in simulation units, see Ref. [45]). Data were measured for glasses of various sizes N and parent temperatures T_p as indicated by the legend. (b) Same phonon-band widths $\Delta\omega$ as reported in (a), this time plotted against the rescaled frequency $\omega\sqrt{n_z}/\sqrt{N}$. The continuous lines are fits to Eq. (3) from which we estimate $\chi(T_p)$.

strength of finite-size effects. For our spectral-width calculations described below, it is necessary to employ somewhat large systems to cleanly estimate the widths of the lowest-frequency phonon bands in solids quenched from high parent temperatures. The system sizes we employed for these calculations per each parent temperature are described in the legend of Fig. 2(a) below.

B. Spectral widths $\Delta\omega$ of discrete phonon-bands

Phonon band widths $\Delta\omega$ for each T_p-ensemble were estimated as follows:

(1) We performed a partial diagonalization of the Hessian matrix $\boldsymbol{H} \equiv \frac{\partial^2 U}{\partial \boldsymbol{x}\partial \boldsymbol{x}}$ for at least 50 independent configurations for each T_p ensemble to obtain the vibrational eigenfrequencies ω_ℓ (all particle masses in our model are set to unity) and their associated eigenmodes $\boldsymbol{\Psi}^{(\ell)}$.

(2) We filtered eigenfrequencies ω_ℓ according to the participation ratio $e(\boldsymbol{\Psi}^{(\ell)}) \equiv [N \sum_i (\boldsymbol{\Psi}_i^{(\ell)} \cdot \boldsymbol{\Psi}_i^{(\ell)})^2]^{-1}$ of their corresponding eigenmodes $\boldsymbol{\Psi}^{(\ell)}$, as also done in Refs. [25,30]. In our analyses, we only considered eigenmodes $\boldsymbol{\Psi}^{(\ell)}$
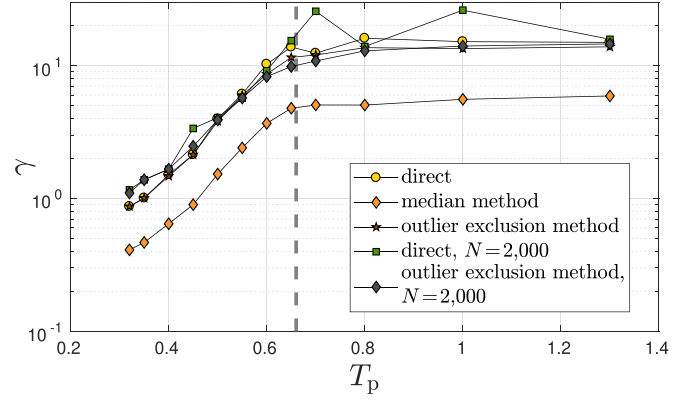

FIG. 3. Comparison between the direct calculation of γ (via sample-to-sample statistics), and the two estimation methods as described in the text for computer glasses of $N = 16\,000$ particles. The vertical dashed line marks the crossover temperature T_X [46], which coincides with the onset of the high-T_p plateau of γ. Also plotted are direct measurements and the outlier exclusion estimations of γ for systems of $N = 2000$ particles (using the same ensemble sizes as the $N = 16\,000$ systems), which are much noisier [15]. We find that, for $N = 16\,000$, the outlier exclusion method estimation follows closely the direct measurement at low T_p, and is roughly 55% higher than the median-based estimation throughout the studied T_p range. We therefore adopt the outlier-exclusion estimate of γ in what follows.

with $e(\boldsymbol{\Psi}^{(\ell)}) > 0.03$ to prevent low-frequency quasilocalized modes from affecting our estimations of phonon-band widths.

(3) We fitted a Gaussian to each peak pertaining to individual phonon bands, as done and explained in Ref. [25]. The spectral widths $\Delta\omega$ were taken as the standard deviation (std) obtained from those Gaussian fits.

In Fig. 2, we present our measurements of our different T_p glasses' phonon-band widths $\Delta\omega$. In Fig. 2(a), we present the raw data obtained from the Gaussian fits as explained above. In Fig. 2(b), we plot the same data as shown in Fig. 2(a), this time against the rescaled frequency $\omega\sqrt{n_z}/\sqrt{N}$. For each T_p, we fit the data following Eq. (2)—represented by the continuous $\propto \omega$ lines in Fig. 2(b)—to obtain an estimation of $\chi(T_p)$ in accordance with its definition in Eq. (3).

C. Sample-to-sample μ fluctuations

Having at hand estimations for χ, we now turn to estimating γ via the sample-to-sample fluctuations $\Delta\mu$ of the shear modulus μ. Support for the equivalence between these procedures has been presented recently in Ref. [44]. To this aim, we first stress that the sample-to-sample distribution $p(\mu; N)$ of glasses of size N shows strong finite-size effects, as discussed at length in Refs. [8,15]. In particular, in small glass samples quenched from high parent temperatures, some occurrences of anomalously large fluctuations of μ are often observed, rendering a clean estimation of the variance $(\Delta\mu)^2$ difficult. This finite-size effect—which is also demonstrated in Fig. 3 below—is likely related to the deviations from the ω^4 law observed in small computer glasses instantaneously quenched from high parent temperatures [47].

To overcome this potential difficulty, we adopt and compare between two approaches introduced in Refs. [15,45], respectively:

(1) We follow the procedure described in Ref. [15] to remove outliers from each data set $\{\mu_i\}$ pertaining to each parent temperature T_p, as follows: For each data point μ_i, we calculate $\text{std}(\mu)$ for all *other* data points $j \neq i$, namely, under the *exclusion* of μ_i. We then identify the data point whose exclusion leads to the *largest* variation of $\text{std}(\mu)$ amongst all other data points; if that (largest) variation with respect to the original (unfiltered) value of $\text{std}(\mu)$ exceeds 1%, we permanently remove the identified data point from the total data set. This procedure is repeated until the variation of the standard deviation $\text{std}(\mu)$ under exclusion of any single data point is smaller than 1%. This method is referred to below as the *outlier exclusion* method.

(2) In Ref. [45], a measure of the width of the sample-to-sample distribution $p(\mu)$ was defined as the square-root of the *median* (instead of the mean, as done for obtaining $\text{std}(\mu)$) of the squared fluctuations $(\mu_i - \langle\mu\rangle)^2$ about the ensemble-mean $\langle\mu\rangle$. We refer to this method as the *median* method. Notice that here we report the median of $(\mu_i - \langle\mu\rangle)^2$ rather than the square-root of the median as reported in Ref. [45].

In Fig. 3, we compare our estimations of γ using the direct calculation and the two analysis schemes described above (outlier-exclusion and median methods). We find that the outlier-exclusion method results in slightly lower values of γ for high T_p glasses. Importantly, we reiterate that our calculations are performed on ensembles of 2000 glasses of $N = 16\,000$ particles, explaining why the difference between the direct calculation and the outlier elimination method are quite underwhelming. In Fig. 3, we also show the direct calculation of γ for glasses of $N = 2000$ particles, which is substantially noisier, see Ref. [15] for a related discussion. We further note that the data obtained with the outlier exclusion method are roughly proportional to the estimations of γ based on the median of fluctuations as described above, which is much less sensitive to outliers. For these reasons, we opt for the outlier-exclusion method to estimate γ in what follows below. Finally, note that the crossover temperature T_χ [46], marked by vertical dashed line in Fig. 3, appears to coincide with the onset of the high-T_p plateau of γ. The physical significance and relevance of this interesting observation will be discussed elsewhere.

With estimations of $\gamma(T_p)$ and $\chi(T_p)$ at hand, we parametrically plot the two quantifiers against each other in Fig. 4 to find that $\gamma \sim \chi^2$, as predicted by our scaling theory in Sec. II.

IV. MECHANICAL DISORDER NEAR THE UNJAMMING POINT

Up to now we demonstrated the validity of our main prediction in Eq. (10) for computer glasses quenched from a melt, cf. Fig. 4. Our prediction, however, is expected to be generally valid for a broader class of disordered solids. This is demonstrated in this section.

The unjamming transition is a mechanical instability observed upon decompressing athermal packings of frictionless soft spheres [36,37,48,49]. Growing length scales and correlation volumes are known to emerge in these systems as their
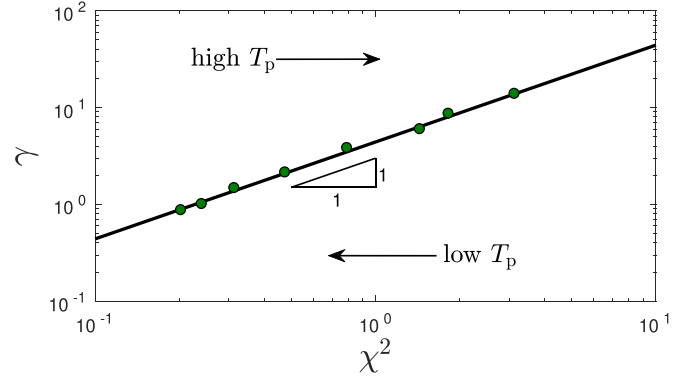

FIG. 4. Parametric plot of $\gamma(T_p)$ vs $\chi^2(T_p)$ obtained as explained in the text. The main result of this paper is that $\gamma \sim \chi^2$, as predicted by our scaling theory in Eq. (10).

confining pressure is reduced toward zero [50–55]. The key microscopic parameter controlling the mechanical behavior of low-pressure soft-sphere packings is the coordination Z, which represents the number of interactions per particle. In particular, scaling laws of elastic moduli [56,57] and length scales [50,51,53–55] with the difference $\delta Z \equiv Z - Z_c$ are known to emerge, where the critical coordination $Z_c = 2\bar{d}$—known as the Maxwell threshold [58]—is reached in the limit of vanishing confining pressure.

How do the interrelated mechanical disorder quantifiers discussed here behave near the unjamming point? In Refs. [59,60], the spectral widths of acoustic excitations are obtained using Effective Medium calculations on disordered Hookean spring networks of coordination Z; the key result relevant to the present discussion is the scaling $\Delta\omega \sim \omega^4/\delta Z^{5/2}$ (in three dimensions), implying together with Eq. (9) and $\omega_0 \sim \sqrt{\mu} \sim \sqrt{\delta Z}$ [57] that $\gamma \sim 1/\delta Z$. This result is consistent with numerical data from simulations of soft-sphere packings put forward in Ref. [52], where it was shown that the sample-to-sample shear modulus distribution collapses for different pressures and system sizes if it is considered for systems with constant $N\delta Z$, implying again that $\gamma \sim 1/\delta Z$ near the unjamming point. We note, however, that the numerical results of Ref. [6] for wave attenuation rates in soft-sphere packings near the unjamming point do not agree with the Effective Medium prediction, as discussed in that same work.

If the relation $\gamma \sim \chi^2$ is general, it should hold in systems near the unjamming transition as well. Here, we test this scaling relation by measuring the broadening of discrete, low-frequency phonon-bands of disordered spring networks in two dimensions. Our networks' geometry was first derived from the contact network of disordered soft-disc packings, and their coordination Z was reduced toward Z_c using an edge-dilution scheme described in the Appendix, which minimizes fluctuations of the angles formed by edges around nodes. The results are presented in Fig. 5; we find that $\chi \sim 1/\sqrt{\delta Z}$, in agreement with our main theoretical prediction.

V. CONCLUDING REMARKS AND PROSPECTS

In this paper, we have discussed two broadly applicable and dimensionless quantifiers of mechanical disorder. The first
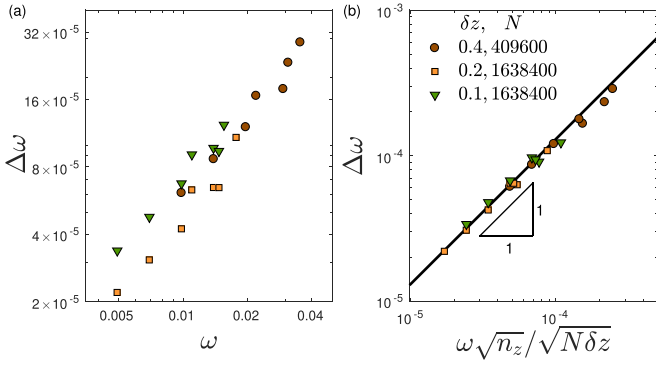
FIG. 5. Phonon-band widths $\Delta\omega$ measured in disordered spring networks in two dimensions, see text and Appendix for details. $\Delta\omega$ is plotted against the frequency ω in panel (a), and against the rescaled frequency $\omega\sqrt{n_z}/\sqrt{\delta ZN} \sim \chi\omega\sqrt{n_z}/\sqrt{N}$ in panel (b). The data collapse implies that $\chi \sim 1/\sqrt{\delta Z} \sim \sqrt{\gamma}$, strengthening the generality of the scaling relation between the mechanical disorder quantifiers γ and χ.

quantifier, χ, is related to the spectral broadening of discrete phonon bands seen in the low-frequency spectra of finite-size computer glasses, as shown in Figs. 1(a) and 1(c). The second quantifier, γ, is known as the disorder parameter in FET [14,17–20] and plays a key role in determining the spectral widths of acoustic excitations in the thermodynamic limit. Our main result—$\gamma \sim \chi^2$—was validated (in Fig. 4) against extensive computer simulations of glasses quenched from a broad range of parent temperatures T_p. It was also validated (in Fig. 5) against computer simulations of disordered spring networks approaching the unjamming transition.

To assess the value of γ—which characterizes the relative width of the distribution of coarse-grained elastic moduli *fields* in disordered media [see Eq. (8)]—we employed sample-to-sample statistics instead of spatial coarse-graining procedures. The equivalence of these two approaches to evaluating γ was recently argued for in Ref. [44] based on detailed analyses of computer glasses. A deeper understanding of this

equivalence and its further reinforcement is left for future investigations.

In Figs. 1(a)–1(c), we presented data that indicate that the prefactor A_g of the universal $\propto\omega^4$ nonphononic VDoS correlates with the mechanical disorder quantifiers γ and χ discussed in this paper. It is natural to expect that systems rich with soft nonphononic modes—as indicated by a large (dimensionless) prefactor $A_g\omega_0^5$—would also have relatively large spatial fluctuations of their coarse-grained shear modulus fields. Indeed, in Ref. [13] it was argued that $A_g\omega_0^5 \sim \gamma^{5/3}$ in three-dimensional glasses [61], based on scaling arguments.

These predictions are tested against our computer glasses data in Fig. 6. In Fig. 6(a), we show the low-frequency VDoS of our computer glasses of different parent temperatures T_p; we obtain estimations of the dimensionless prefactors $A_g\omega_0^5$ by fitting the low-frequency tails to the universal $\sim\omega^4$ law. In Fig. 6(b), we plot the extracted $A_g\omega_0^5$ versus the disorder parameter γ obtained as explained in Sec. III C. We find that the proposed scaling $A_g\omega_0^5 \sim \gamma^{5/3}$ holds over a limited, intermediate range of γ values. As pointed out in Refs. [15,62], $A_g\omega_0^5$ dips downward at the lowest values of γ. In Ref. [62], it was demonstrated that γ varies monotonically with a glassy correlation length ξ_g, which is expected to be bounded from below by an interparticle distance, suggesting a lower bound on γ as well. Relations between the glassy length ξ_g, the disorder parameter γ and the prefactor A_g were suggested, discussed and tested further in Refs. [15,44,54,62]. A complete understanding of the relation between A_g and the disorder quantifiers discussed here is left for future work.

We conclude the discussion with commenting on the experimental accessibility of the mechanical disorder quantifiers discussed in this paper. Spectral widths of acoustic excitations $\Delta\omega(k)$ are related to wave attenuation rates $\Gamma(k)$ as $\Gamma \sim \Delta\omega$, as demonstrated for frequencies $\omega < \omega_†$ using computer simulations in Ref. [25], and for frequencies $\omega > \omega_†$ in Ref. [44]. While longitudinal wave attenuation rates are accessible experimentally [63,64] via high-resolution inelastic x-ray scattering, methods for measuring transverse (shear) waves' attenuation rates well in the Rayleigh scaling regime
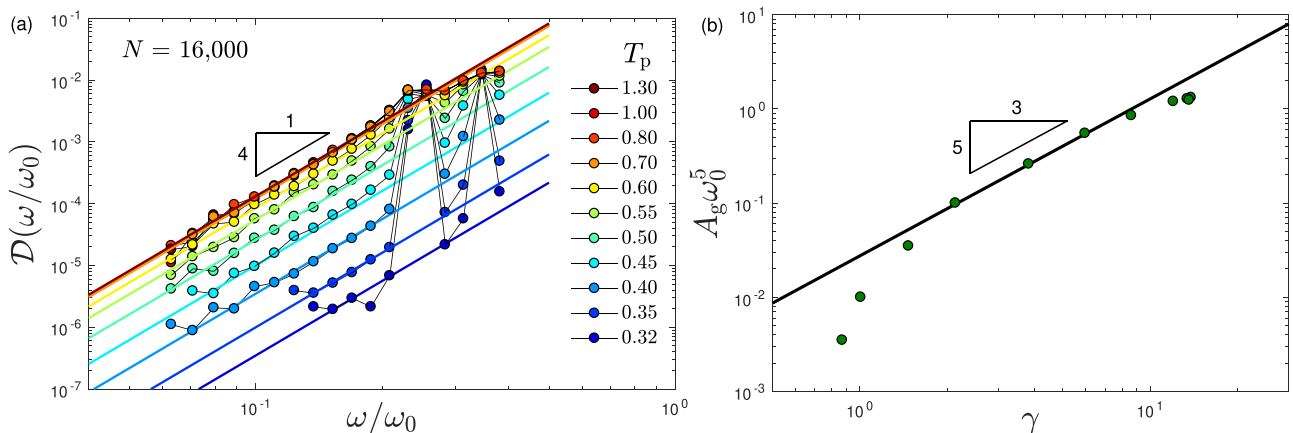

FIG. 6. (a) VDoS of our computer glasses of various T_p as indicated by the legend. The dimensionless prefactors $A_g\omega_0^5$ are estimated by fitting the low frequency tails to the universal quartic law $\propto\omega^4$ of the nonphononic VDoS. The extracted dimensionless prefactors $A_g\omega_0^5$ are then plotted in panel (b) vs. the disorder parameter γ obtained from the sample-to-sample fluctuations of the shear modulus as explained in the text. In Ref. [13] it is argued that $A_g\omega_0^5 \sim \gamma^{5/3}$, as represented by the continuous line.
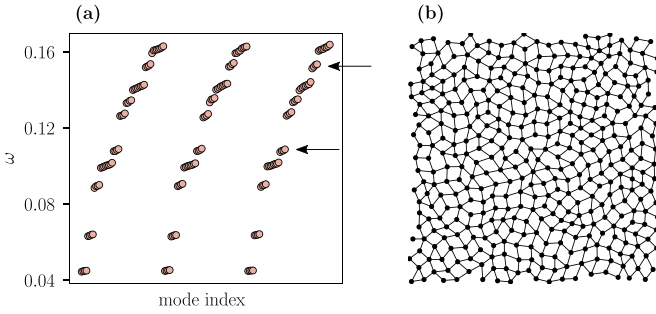
FIG. 7. (a) Lowest-frequency phonon bands of three realizations of spring networks of $N = 1\,638\,400$ nodes with coordination $Z = 4.1$ generated using the algorithm described in the text. Sound waves are marked by arrows. (b) An example of a spring network of $N = 400$ nodes and coordination $Z = 4.1$ generated with the algorithm described here.

($k \lesssim 1\mathrm{nm}^{-1}$) are unfortunately not yet available. In Ref. [65], a measure of local elastic moduli of a metallic glass (amorphous PdCuSi) was obtained using atomic force acoustic microscopy. There, it was reported that $\Delta\mu/\mu \approx 30\%$, where the fluctuations were estimated over lengths of order 10 nm. An important goal of future experiments is to assess and compare the mechanical disorder of laboratory glasses to our measurements of the mechanical disorder of computer glasses on equal footing, in terms of the quantifiers discussed in this paper. An impressive effort in this direction was presented very recently in Ref. [14].

APPENDIX: DISORDERED SPRING NETWORKS

We created two-dimensional disordered networks of Hookean springs by adopting the contact networks of the soft-disc glasses described and studied in Ref. [24]. The particle centers of the original glass are set to be the networks' nodes, and an edge is placed between each pair of interacting particles in the original glass. The coordination of these initial networks is $Z \approx 6.5$. We employed the edge-dilution algorithm described below to remove edges until the target coordinations $Z = 4.4, 4.2, 4.1$ were reached. Each edge of the remaining network is then replaced by a *relaxed* Hookean spring (of unit stiffness), i.e., the spring's rest length is set to the original distance between the pair of nodes it is connected to. An example of a network produced by our algorithm is shown in Fig. 7(b).

The low-frequency spectrum of the disordered networks produced by our scheme—provided the system is large enough—consists solely of phonons, as demonstrated in Fig. 7(a). This is a nontrivial feature of our scheme. We tested
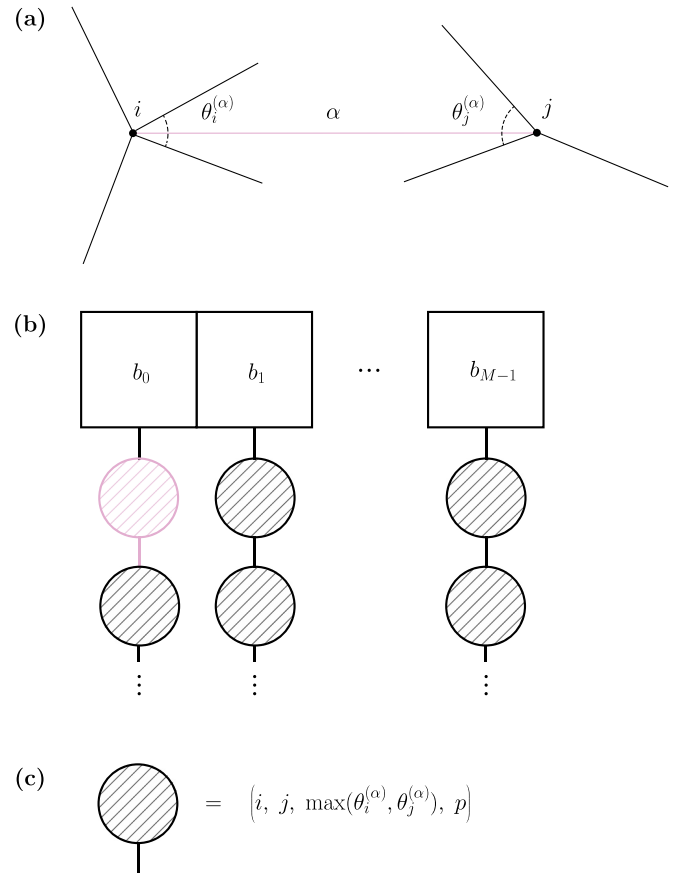

FIG. 8. (a) When an edge α is removed, two remaining angles $\theta_i^{(\alpha)}$ and $\theta_j^{(\alpha)}$ are formed at nodes i and j. In each iteration of the algorithm, we aim to remove the edge whose removal forms the *smallest* remaining angles. (b) Illustration of the key data structure of the algorithm; upon initialization, all edges of the initial network are stored in b—an array of linked lists—so b_i contains a linked list of edges with $\frac{2\pi i}{M} < \max(\theta_i^{(\alpha)}, \theta_j^{(\alpha)}) < \frac{2\pi(i+1)}{M}$. The edge targeted for removal is shown in pink. (c) An element of a linked list contains an edge α specified by the two nodes i and j, the largest bond angle that would open up in case of its removal, and a pointer p to the next element of the linked list.

other edge-dilution schemes aimed at minimizing local coordination fluctuations. The low-frequency spectrum of spring networks with small δZ produced by these other schemes usually features localized, nonphononic soft vibrations, in addition to phonons. Since the low-frequency spectrum of the spring networks produced by our algorithm consists solely of phonons, we could directly measure the spectral width of phonon bands by calculating the standard deviation of the vibrational frequencies of each band.

Bond-dilution algorithm

We introduce an algorithm [66] that iteratively removes edges from a two-dimensional network, based on the network's geometry. To explain how the algorithm works, we refer readers to the illustration in Fig. 8(a); removing the edge labeled α between two nodes i and j creates two *remaining* angles $\theta_i^{(\alpha)}$ and $\theta_j^{(\alpha)}$. In each edge-removal iteration of our

algorithm, the next edge to be removed is the one whose larger (out of two) associated remaining angle (as defined above) is *minimal*, across all edges.

The algorithm consists of a preprocessing step and a removal step. The preprocessing step creates an array of M linked-lists, denoted by b. The links of each linked list represent edges; each link representing an edge stores the larger of the two remaining angles that would be formed upon removal of that edge, namely, $\theta^{(\alpha)} \equiv \max(\theta_i^{(\alpha)}, \theta_j^{(\alpha)})$. Each linked list b_ℓ holds the edges α whose $\theta^{(\alpha)}$ are equal up to $2\pi/M$, namely, those that satisfy $\frac{2\pi\ell}{M} < \theta^{(\alpha)} < \frac{2\pi(\ell+1)}{M}$. This data structure is explained in Fig. 8(b).

To find the edge that opens up the smallest bond-angle (up to accuracy $2\pi/M$), we simply find the first element of b that contains a nonempty linked list and remove the edge that is stored in the head of that linked list [shown in pink in Fig. 8(b)]. The second element of the linked list becomes its new head. To remove subsequent edges, we simply repeat this procedure, emptying the linked lists in the array b from left to right.

Importantly, when a link is considered for removal, it is necessary to check if the originally stored $\theta^{(\alpha)}$ is still accurate, since previous edge removals might have increased it. If $\theta^{(\alpha)}$ is unchanged, we remove the edge. If $\theta^{(\alpha)}$ has changed due to other edge removals, we remove its link and reinsert it at the head of the linked list in b corresponding to the updated remaining angle $\theta^{(\alpha)}$. The reason we can traverse b from left to right is that $\theta^{(\alpha)}$ can only *increase* when we remove other edges $\neq \alpha$. To create the networks used in this paper, we chose $M = 10^4$.

[1] A. Cavagna, Supercooled liquids for pedestrians, Phys. Rep. **476**, 51 (2009).

[2] S. Sakaguchi, S. Todoroki, and T. Murata, Rayleigh scattering in silica glass with heat treatment, J. Non-Cryst. Solids **220**, 178 (1997).

[3] J. Pan, Y. X. Wang, Q. Guo, D. Zhang, A. L. Greer, and Y. Li, Extreme rejuvenation and softening in a bulk metallic glass, Nat. Commun. **9**, 560 (2018).

[4] X. Bian, G. Wang, H. Chen, L. Yan, J. Wang, Q. Wang, P. Hu, J. Ren, K. Chan, N. Zheng, A. Teresiak, Y. Gao, Q. Zhai, J. Eckert, J. Beadsworth, K. Dahmen, and P. Liaw, Manipulation of free volumes in a metallic glass through Xe-ion irradiation, Acta Mater. **106**, 66 (2016).

[5] J. Shen, D. J. Green, R. E. Tressler, and D. L. Shelleman, Stress relaxation of a soda lime silicate glass below the glass transition temperature, J. Non-Cryst. Solids **324**, 277 (2003).

[6] H. Mizuno and A. Ikeda, Phonon transport and vibrational excitations in amorphous solids, Phys. Rev. E **98**, 062612 (2018).

[7] L. Wang, G. Szamel, and E. Flenner, Sound attenuation in finite-temperature stable glasses, Soft Matter **16**, 7165 (2020).

[8] G. Kapteijns, D. Richard, E. Bouchbinder, and E. Lerner, Elastic moduli fluctuations predict wave attenuation rates in glasses, J. Chem. Phys. **154**, 081101 (2021).

[9] R. G. Ross, Thermal conductivity and disorder in nonmetallic materials, Phys. Chem. Liq. **23**, 189 (1991).

[10] M. J. Demkowicz and A. S. Argon, Liquidlike atomic environments act as plasticity carriers in amorphous silicon, Phys. Rev. B **72**, 245205 (2005).

[11] J. Ketkaew, W. Chen, H. Wang, A. Datye, M. Fan, G. Pereira, U. D. Schwarz, Z. Liu, R. Yamada, W. Dmowski, M. D. Shattuck, C. S. O'Hern, T. Egami, E. Bouchbinder, and J. Schroers, Mechanical glass transition revealed by the fracture toughness of metallic glasses, Nat. Commun. **9**, 3271 (2018).

[12] E. Y. Lin and R. A. Riggleman, Distinguishing failure modes in oligomeric polymer nanopillars, Soft Matter **15**, 6589 (2019).

[13] D. Richard, E. Lerner, and E. Bouchbinder, Brittle to ductile transitions in glasses: Roles of soft defects and loading geometry, arXiv:2103.05258.

[14] Z. Pan, O. Benzine, S. Sawamura, R. Limbach, A. Koike, T. Bennett, G. Wilde, W. Schirmacher, and L. Wondraczek, Disor-der classification of the vibrational spectra of modern glasses, ChemRxiv (2021).

[15] K. González-López, M. Shivam, Y. Zheng, M. P. Ciamarra, and E. Lerner, Mechanical disorder of sticky-sphere glasses. I. Effect of attractive interactions, Phys. Rev. E **103**, 022605 (2021).

[16] D. Richard, K. González-López, G. Kapteijns, R. Pater, T. Vaknin, E. Bouchbinder, and E. Lerner, Universality of the Nonphononic Vibrational Spectrum Across Different Classes of Computer Glasses, Phys. Rev. Lett. **125**, 085502 (2020).

[17] W. Schirmacher, Thermal conductivity of glassy materials and the boson peak, Europhys. Lett. **73**, 892 (2006).

[18] W. Schirmacher, G. Ruocco, and T. Scopigno, Acoustic Attenuation in Glasses and Its Relation With the Boson Peak, Phys. Rev. Lett. **98**, 025501 (2007).

[19] W. Schirmacher, Some comments on fluctuating-elasticity and local oscillator models for anomalous vibrational excitations in glasses, J. Non-Cryst. Solids **357**, 518 (2011).

[20] W. Schirmacher and G. Ruocco, Heterogeneous elasticity: The tale of the boson peak, arXiv:2009.05970.

[21] A. Widmer-Cooper, H. Perry, P. Harrowell, and D. R. Reichman, Irreversible reorganization in a supercooled liquid originates from localized soft modes, Nat. Phys. **4**, 711 (2008).

[22] H. Tong and N. Xu, Order parameter for structural heterogeneity in disordered solids, Phys. Rev. E **90**, 010401(R) (2014).

[23] R. Milkus and A. Zaccone, Local inversion-symmetry breaking controls the boson peak in glasses and crystals, Phys. Rev. B **93**, 094204 (2016).

[24] E. Lerner and E. Bouchbinder, A characteristic energy scale in glasses, J. Chem. Phys. **148**, 214502 (2018).

[25] E. Bouchbinder and E. Lerner, Universal disorder-induced broadening of phonon bands: From disordered lattices to glasses, New J. Phys. **20**, 073022 (2018).

[26] C. Rainone, E. Bouchbinder, and E. Lerner, Pinching a glass reveals key properties of its soft spots, Proc. Natl. Acad. Sci. USA **117**, 5228 (2020).

[27] D. Richard, M. Ozawa, S. Patinet, E. Stanifer, B. Shang, S. A. Ridout, B. Xu, G. Zhang, P. K. Morse, J.-L. Barrat, L. Berthier, M. L. Falk, P. Guan, A. J. Liu, K. Martens, S. Sastry, D. Vandembroucq, E. Lerner, and M. L. Manning, Predicting plasticity in disordered solids from structural indicators, Phys. Rev. Materials **4**, 113609 (2020).

[28] The longitudinal to transverse wave-speeds ratio of our $T_p = 0.4$ glasses is ≈ 2.5; as a result, the six lowest-frequency phonon bands seen in Fig. 1(a) pertain to transverse phonons, whereas the first band of longitudinal phonons is submerged at the upper-edge of the sixth band of transverse phonons.

[29] E. Lerner, G. Düring, and E. Bouchbinder, Statistics and Properties of Low-Frequency Vibrational Modes in Structural Glasses, Phys. Rev. Lett. **117**, 035501 (2016).

[30] H. Mizuno, H. Shiba, and A. Ikeda, Continuum limit of the vibrational properties of amorphous solids, Proc. Natl. Acad. Sci. USA **114**, E9767 (2017).

[31] G. Kapteijns, E. Bouchbinder, and E. Lerner, Universal Non-Phononic Density of States in 2D, 3D and 4D Glasses, Phys. Rev. Lett. **121**, 055501 (2018).

[32] L. Wang, A. Ninarello, P. Guan, L. Berthier, G. Szamel, and E. Flenner, Low-frequency vibrational modes of stable glasses, Nat. Commun. **10**, 26 (2019).

[33] A. Ninarello, L. Berthier, and D. Coslovich, Models and Algorithms for the Next Generation of Glass Transition Studies, Phys. Rev. X **7**, 021039 (2017).

[34] N.-H. Tsai, F. F. Abraham, and G. Pound, The structure and thermodynamics of binary microclusters: A Monte Carlo simulation, Surf. Sci. **77**, 465 (1978).

[35] D. Gazzillo and G. Pastore, Equation of state for symmetric non-additive hard-sphere fluids: An approximate analytic expression and new Monte Carlo results, Chem. Phys. Lett. **159**, 388 (1989).

[36] A. J. Liu, S. R. Nagel, W. Van Saarloos, and M. Wyart, The jamming scenario—an introduction and outlook, in *Dynamical Heterogeneities in Glasses, Colloids, and Granular Media* (Oxford University Press, Oxford, England, 2011).

[37] M. van Hecke, Jamming of soft particles: Geometry, mechanics, scaling and isostaticity, J. Phys.: Condens. Matter **22**, 033101 (2010).

[38] Here we assume that the spatial fluctuations of coarse-grained shear modulus fields are equivalent to its sample-to-sample fluctuations, as demonstrated recently [44].

[39] N. W. Ashcroft and N. D. Mermin, *Solid State Physics* (Saunders College Publishing, Philadelphia, 1976).

[40] A. Moriel, G. Kapteijns, C. Rainone, J. Zylberg, E. Lerner, and E. Bouchbinder, Wave attenuation in glasses: Rayleigh and generalized-Rayleigh scattering scaling, J. Chem. Phys. **151**, 104503 (2019).

[41] P. G. Klemens, The thermal conductivity of dielectric solids at low temperatures (theoretical), Proc. R. Soc. A **208**, 108 (1951).

[42] L. Rayleigh, On the scattering of light by small particles, Philos. Mag. **41**, 447 (1871).

[43] L. Wang, L. Berthier, E. Flenner, P. Guan, and G. Szamel, Sound attenuation in stable glasses, Soft Matter **15**, 7018 (2019).

[44] S. Mahajan and M. P. Ciamarra, Unifying description of the vibrational anomalies of amorphous materials, arXiv:2106.04868.

[45] E. Lerner, Mechanical properties of simple computer glasses, J. Non-Cryst. Solids **522**, 119570 (2019).

[46] K. González-López and E. Lerner, An energy-landscape-based crossover temperature in glass-forming liquids, J. Chem. Phys. **153**, 241101 (2020).

[47] E. Lerner, Finite-size effects in the nonphononic density of states in computer glasses, Phys. Rev. E **101**, 032120 (2020).

[48] C. S. O'Hern, L. E. Silbert, A. J. Liu, and S. R. Nagel, Jamming at zero temperature and zero applied stress: The epitome of disorder, Phys. Rev. E **68**, 011306 (2003).

[49] A. J. Liu and S. R. Nagel, The jamming transition and the marginally jammed solid, Annu. Rev. Condens. Matter Phys. **1**, 347 (2010).

[50] L. E. Silbert, A. J. Liu, and S. R. Nagel, Vibrations and Diverging Length Scales Near the Unjamming Transition, Phys. Rev. Lett. **95**, 098301 (2005).

[51] E. Lerner, E. DeGiuli, G. During, and M. Wyart, Breakdown of continuum elasticity in amorphous solids, Soft Matter **10**, 5085 (2014).

[52] C. P. Goodrich, S. Dagois-Bohy, B. P. Tighe, M. van Hecke, A. J. Liu, and S. R. Nagel, Jamming in finite systems: Stability, anisotropy, fluctuations, and scaling, Phys. Rev. E **90**, 022138 (2014).

[53] K. Baumgarten, D. Vågberg, and B. P. Tighe, Nonlocal Elasticity Near Jamming in Frictionless Soft Spheres, Phys. Rev. Lett. **118**, 098001 (2017).

[54] M. Shimada, H. Mizuno, M. Wyart, and A. Ikeda, Spatial structure of quasilocalized vibrations in nearly jammed amorphous solids, Phys. Rev. E **98**, 060901(R) (2018).

[55] D. Hexner, A. J. Liu, and S. R. Nagel, Two Diverging Length Scales in the Structure of Jammed Packings, Phys. Rev. Lett. **121**, 115501 (2018).

[56] M. Wyart, On the rigidity of amorphous solids, Ann. Phys. **30**, 1 (2005).

[57] W. G. Ellenbroek, Z. Zeravcic, W. van Saarloos, and M. van Hecke, Non-affine response: Jammed packings vs. spring networks, Europhys. Lett. **87**, 34004 (2009).

[58] J. C. Maxwell, On the calculation of the equilibrium and stiffness of frames, Philos. Mag. **27**, 294 (1864).

[59] M. Wyart, Scaling of phononic transport with connectivity in amorphous solids, Europhys. Lett. **89**, 64001 (2010).

[60] E. DeGiuli, A. Laversanne-Finot, G. During, E. Lerner, and M. Wyart, Effects of coordination and pressure on sound attenuation, boson peak and elasticity in amorphous solids, Soft Matter **10**, 5628 (2014).

[61] Generalizing the argument of Ref. [13] to general dimension $đ$, one expects $A_g \omega_0^5 \sim \gamma^{5/d}$.

[62] K. González-López, E. Bouchbinder, and E. Lerner, Does a universal lower bound on glassy mechanical disorder exist? arXiv:2012.03634.

[63] B. Ruta, G. Baldi, F. Scarponi, D. Fioretto, V. M. Giordano, and G. Monaco, Acoustic excitations in glassy sorbitol and their relation with the fragility and the boson peak, J. Chem. Phys. **137**, 214502 (2012).

[64] G. Baldi, V. M. Giordano, B. Ruta, R. Dal Maschio, A. Fontana, and G. Monaco, Anharmonic Damping of Terahertz Acoustic Waves in a Network Glass and Its Effect on the Density of Vibrational States, Phys. Rev. Lett. **112**, 125502 (2014).

[65] H. Wagner, D. Bedorf, S. Küchemann, M. Schwabe, B. Zhang, W. Arnold, and K. Samwer, Local elastic properties of a metallic glass, Nat. Mater. **10**, 439 (2011).

[66] Our algorithm is an adaptation of an algorithm developed by J. Zylberg.